

REMAA: Reconfigurable Pixel Antenna-Based Electronic Movable-Antenna Arrays for Multiuser Communications

Kangjian Chen¹, Graduate Student Member, IEEE, Chenhao Qi², Senior Member, IEEE, Yujing Hong³, Graduate Student Member, IEEE, and Chau Yuen⁴, Fellow, IEEE

Abstract—This paper investigates reconfigurable pixel antenna (RPA)-based electronic movable antennas (REMA) for multiuser communications. First, we model each REMA as an antenna with a set of predefined and discrete selectable radiation positions within the radiating region. Considering the trade-off between performance and cost, we propose partially-connected and fully-connected RPA-based electronic movable-antenna arrays (PC/FC-REMAA). Then, we formulate a multiuser sum-rate maximization problem subject to the power and hardware constraints of the PC/FC-REMAA. To solve this problem, we propose a two-step multiuser beamforming and antenna selection scheme. In addition, we revisit mechanical movable antennas (MMAs) to establish a benchmark for evaluating the performance of REMA-enabled multiuser communications. Finally, we analyze the performance gap between REMAs and MMAs. Based on Fourier analysis, we derive the maximum power loss of REMAs compared to MMAs for any given position interval. Specifically, we show that REMAs lose at most 3.25% power relative to MMAs when the position interval is one-tenth of the wavelength. Simulation results demonstrate the effectiveness of the proposed methods.

Index Terms—Fluid antenna, joint beamforming and antenna selection, movable antennas, multiuser communications, sum-rate maximization.

I. INTRODUCTION

WITH the emergence of applications such as the Internet of Things, smart homes, and industrial automation, wireless communications face increasing performance demands, including higher data rates, broader coverage, lower power consumption, and greater adaptability [2], [3]. As a

result, enhancing the capability, efficiency, and flexibility of wireless communication systems has become a primary focus of current research.

As the fundamental medium for information transmission, wireless channels crucially influence communication performance [3], [4]. Thus, optimizing channel usage has become a key research focus. For example, conventional MIMO communications enhance transmission performance by exploiting the inherent degrees of freedom of channels [5]. Specifically, spatial multiplexing improves communication rates by enabling parallel transmission of multiple data streams while spatial diversity enhances communication reliability by exploiting the independent transmission of multiple channel paths. To further extend the spatial dimensions available for communication, massive MIMO systems have been developed by substantially increasing the number of antennas relative to conventional MIMO [6], [7], [8], which changes the channel characteristics and expands the flexibility available for signal design. In this regard, beamforming is performed to adapt to the channel characteristics and exploit this additional flexibility [9], [10], [11]. By optimizing the utilization of channels, conventional MIMO and massive MIMO significantly enhance communication performance.

Notably, both the conventional and massive MIMO typically employ fixed-position antennas (FPAs), which limits their design flexibility. Specifically, the received signal power varies across the reception region due to the interference among signals from multiple paths. Consequently, the antenna positions can significantly impact communication performance, as they influence the strengths of received signal powers. In the case of FPAs, the received power of the antennas remains fixed under given channel conditions and cannot be enhanced through optimization, thereby limiting their communication performance. To address this issue, the antenna selection (AS) has been developed [12], [13], [14]. By deploying a large number of candidate antennas and selecting part of them for wireless communication, AS can adapt to instantaneous channel state information, thus overcoming the limitations of FPAs. Despite its advantages, AS faces two main challenges. On the one hand, to fully exploit the wireless channel, AS requires the deployment of a large number of antennas, which incurs significant hardware costs. Additionally, the physical size constraints of the antennas impose a minimum spacing

Received 13 March 2025; revised 2 June 2025; accepted 14 July 2025. Date of publication 24 July 2025; date of current version 14 November 2025. This work was supported in part by the National Natural Science Foundation of China under Grants 624B2035 and U22B2007, in part by the National Key Research and Development Program of China under Grant 2021YFB2900404, in part by the Ministry of Education, Singapore, under its MOE Tier 2 (Award number T2EP50124-0032), in part by the SEU Innovation Capability Enhancement Plan for Doctoral Students under Grant CXJH_SEU 25019. An earlier version of this paper was presented in part at the IEEE 26th International Workshop on Signal Processing and Artificial Intelligence in Wireless Communications (SPAWC), Surrey, U.K., July 2025 [1]. The associate editor coordinating the review of this article and approving it for publication was M. Hua. (Corresponding author: Chenhao Qi.)

Kangjian Chen and Chenhao Qi are with the School of Information Science and Engineering, Southeast University, Nanjing 210096, China (e-mail: kjchen@seu.edu.cn; qch@seu.edu.cn).

Yujing Hong and Chau Yuen are with the School of Electrical and Electronics Engineering, Nanyang Technological University, Singapore 639798 (e-mail: yujing001@e.ntu.edu.sg; chau.yuen@ntu.edu.sg).

Digital Object Identifier 10.1109/TCOMM.2025.3592593

0090-6778 © 2025 IEEE. All rights reserved, including rights for text and data mining, and training of artificial intelligence and similar technologies. Personal use is permitted, but republication/redistribution requires IEEE permission.

See <https://www.ieee.org/publications/rights/index.html> for more information.

Authorized licensed use limited to: Southeast University. Downloaded on November 14, 2025 at 01:42:56 UTC from IEEE Xplore. Restrictions apply.

between candidate antennas, limiting AS to exploiting channels of specific discrete locations for wireless communications.

To address these challenges, recent research has explored novel methods for achieving flexible mobility of radiating elements, including the use of movable antennas (MAs), fluid antennas (FAs) and flexible intelligent metasurfaces (FIMs) [15], [16], [17], [18], [19], [20]. The key advantage of MAs/FAs/FIMs lies in their ability to move freely within a defined spatial region. Compared to FPAs, MAs/FAs/FIMs provide greater design flexibility by enabling the joint optimization of radiating element positions and beamforming vectors. Compared to AS, MAs/FAs/FIMs allow more flexible adjustment of radiating element positions, leading to greater improvements in communication performance.

Due to the significant potential of MAs/FAs/FIMs, substantial research efforts have been dedicated to exploring their characteristics [21], [22]. For example, in [21], the modeling and performance analysis of one MA are investigated, which reveals that the multipath channel gain exhibits periodic behavior in a given spatial region under deterministic channels. In [22], the authors analyze the probability density function and cumulative distribution function of the signal envelopes for FAs under spatially correlated Rayleigh fading channels. Beyond these theoretical analyses, extensive research has also explored the practical potential of MAs/FAs/FIMs in wireless communication systems [22], [23], [24], [25], [26], [27]. In [22], an approximate closed-form expression for the outage probability of FA systems is derived, demonstrating that FAs can achieve arbitrarily small outage probabilities. In [23], the authors optimize both the transmit covariance matrices and the antenna position vectors of users to maximize system capacity, showing that FAs can significantly improve the capacity of multiple access channels. In [24], a MIMO communication system with MAs is considered, indicating that MA systems substantially outperform FPA systems in terms of MIMO channel capacity. In [25], multiuser communication with MAs is investigated, revealing that the total transmit power can be significantly reduced compared to conventional FPA systems. In [26] and [27], considering that the motion control of electromechanical devices is constrained by discrete adjustments with finite precision, the authors investigate multiuser communications based on MAs with discrete positions, highlighting the advantages of MAs in practice. In addition to these advancements, the effectiveness of MAs and FAs has also been validated in other systems, including wireless sensing [28], integrated sensing and communications [29], [30], secure wireless communications [31], and symbiotic radio systems [32].

Although extensive research has demonstrated the promising potential of MAs/FAs/FIMs, their practical implementation remains an open issue. Initially, MAs/FAs/FIMs are controlled through mechanical methods, where FAs rely on liquid pumping or pressure regulation to adjust the antenna positions, MAs use mechanical devices such as motors to reposition antenna elements within the transmission region, and FIMs use micro-mechanical mechanisms to reconfigure the positions of the radiating elements. While these methods enable flexible movement of radiating elements, their dependence on mechanical

adjustments results in slow position updates, which renders them unsuitable for rapidly varying channels. Recently, an implementation of MAs/FAs based on reconfigurable pixel antennas (RPAs) is proposed in [33]. By electronically controlling radio frequency (RF) components between pixels, this method enables rapid changes of antenna positions, and offers a feasible solution for the practical realization of MAs/FAs. Another example of employing RPAs to realize MAs/FAs is presented in [34], where a dual-band reconfigurable antenna array is proposed. By reusing millimeter-wave antennas to form sub-6 GHz elements and controlling their interconnections via PIN diodes, this design enables dynamic adjustment of the sub-6 GHz antenna positions while maintaining wireless functionality in both bands.

In this paper, we investigate RPA-based electronic movable antennas (REMA), as proposed in [33], for multiuser sum-rate maximization through joint beamforming and antenna selection. The main contributions of this paper are summarized as follows.

- First, we model each REMA as an antenna with a set of predefined and discrete selectable radiation positions within the radiating region. Considering the trade-off between performance and cost, we propose two types of REMA-based arrays: the partially-connected RPA-based electronic movable-antenna array (PC-REMAA) and fully-connected RPA-based electronic movable-antenna array (FC-REMAA).
- Then, we investigate multiuser communications, where the base station (BS) is equipped with either a PC-REMAA or an FC-REMAA, while users employ FPAs. We formulate a multiuser sum-rate maximization problem subject to power and hardware constraints of the PC-REMAA or FC-REMAA. To solve this problem, we propose a two-step multiuser beamforming and antenna selection (TS-MBAS) scheme. In the first step, we develop a two-loop joint beamforming and antenna selection (TL-JBAS) algorithm. In the second step, we apply the coordinate descent method to further enhance the solution of the TL-JBAS algorithm.
- In addition, we revisit mechanical movable antennas (MMAs) to establish a benchmark for evaluating the performance of REMA-enabled multiuser communications, where MMAs can continuously adjust the positions within the transmission region. We also formulate a sum-rate maximization problem for MMA-enabled multiuser communications and propose an alternating beamforming and antenna position optimization (ABAPO) scheme to solve it.
- Moreover, we analyze the performance gap between REMAs and MMAs. Specifically, we transform the received signal of MMAs into the discrete-time Fourier transform (DTFT) of the channel coefficients. Based on Fourier analysis, we derive the maximum power loss of REMAs compared to MMAs for any given position interval.

The rest of this paper is organized as follows. The electronic movable antennas are introduced in Section II. The system model and problem formulation are presented in Section III.

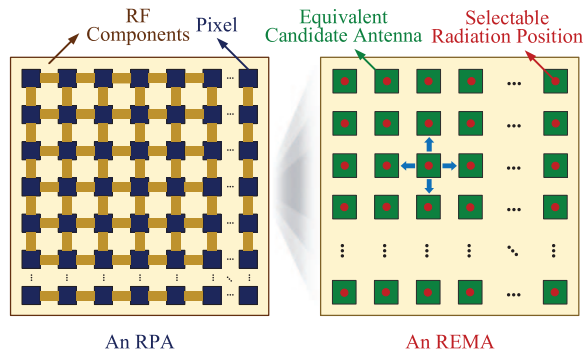


Fig. 1. Illustration of an RPA and an REMA.

The multiuser beamforming and antenna selection for REMAs are developed in Section IV. The revisit of the MMAs is given in Section V. The performance gap analysis between REMAs and MMAs is discussed in Section VI. The proposed methods are evaluated in Section VII, and the paper is concluded in Section VIII.

Notations: Lowercase and uppercase bold symbols denote vectors and matrices, respectively. $[\mathbf{A}]_{m,:}$, $[\mathbf{A}]_{:,n}$, and $[\mathbf{A}]_{m,n}$ denote the m th row, the n th column, and the entry on the m th row and the n th column of a matrix \mathbf{A} . $\mathbf{a} \odot \mathbf{b}$ denotes the Hadamard product of vectors \mathbf{a} and \mathbf{b} . $[\mathbf{a}]_m$ denotes the m th entry of a vector \mathbf{a} . $|\cdot|$, $\|\cdot\|_2$, and $\|\cdot\|_F$ denote the absolute value of a scalar, the ℓ_2 -norm of a vector, and the Frobenius norm of a matrix, respectively. $(\cdot)^T$, $(\cdot)^H$, and $(\cdot)^\dagger$ denote the transpose, Hermitian transpose, and the Moore-Penrose inverse, respectively. \mathbb{C} and $\mathcal{CN}(\cdot)$ denote the set of complex numbers and the complex Gaussian distribution, respectively. $\text{vec}\{\mathbf{A}\}$ denotes the vectorization of the matrix \mathbf{A} . $\mathcal{R}\{a\}$ denotes the real part of a complex number a . \otimes denotes the Kronecker product.

II. ELECTRONIC MOVABLE ANTENNAS

In this section, we first introduce the implementation of REMAs. Then, we discuss the design of antenna arrays using REMAs and propose the PC-REMAA as well as the FC-REMAA.

A. RPA-Based Electronic Movable Antennas

As shown on the left of Fig. 1, in RPAs, the radiating surface is composed of multiple pixel elements, where RF components, such as PIN diodes, are employed between these pixel elements to adjust their connections. As demonstrated in [35] and [36], by dynamically controlling the states of these RF switches, the current distribution across the radiating surface can be altered and thus the radiation pattern can be modified. It is further established in [33] that changing radiation patterns through this method is equivalent to physically moving antenna positions. As a result, RPAs can effectively realize MAs by electronically controlling the RF switches. We refer to antennas implemented in this manner as REMAs.

Based on the implementation of RPAs, we model each REMA as an antenna with a set of predefined and discrete selectable radiation positions within the radiating region, as shown on the right of Fig. 1. Specifically, when an REMA

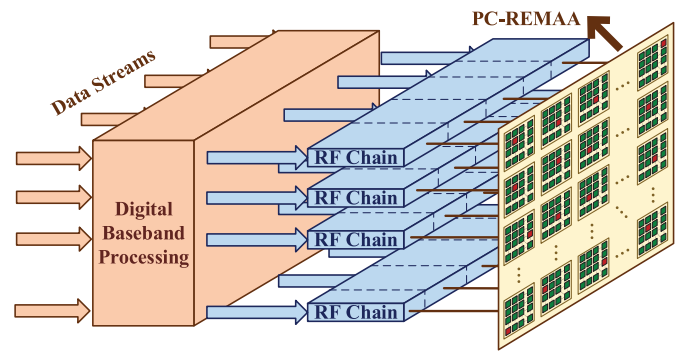


Fig. 2. Illustration of the signal processing architecture for the PC-REMAA.

selects a discrete radiation position, it radiates from that position, which is referred to as a candidate antenna. The parameters of each REMA, including the sizes, positions, numbers, and spacings of candidate antennas, are adjustable during manufacturing, which can be achieved by designing the RPAs with the dedicated efforts of antenna researchers. Once manufactured and deployed, these parameters become fixed and cannot be easily changed. In this work, the candidate antennas are arranged in a uniform planar configuration for simplicity. However, this approach can also be extended to other practical candidate antenna arrangements in future designs.

Remark 1: Unlike conventional AS, which relies on selecting from a predefined set of physically separated antennas with fixed spacing (e.g., half wavelength or larger), the REMA achieves finer position adjustment through coordinated reconfiguration of multiple pixel elements. Specifically, the RPA-based REMA allows candidate antennas to be densely arranged (e.g., 12 ports within half wavelength in [33]), enabling sub-wavelength-level spatial resolution. This is fundamentally distinct from AS, as the REMA dynamically synthesizes radiation patterns by controlling interconnected pixel states rather than merely selecting from isolated antennas. Moreover, when one candidate antenna is selected and other candidate antennas are not, all the pixels are utilized to synthesize the desired radiation pattern, and therefore no hardware resources are wasted. Consequently, the REMAs offer enhanced flexibility in exploiting spatial channel variations while avoiding the hardware complexity and physical size limitations of conventional AS.

B. RPA-Based Electronic Movable-Antenna Arrays

In this part, we discuss the design of electronic movable-antenna arrays with the REMAs.

A straightforward method for constructing an REMAA is to combine multiple REMAs, as depicted in Fig. 2. To achieve a simplified and cost-effective RF architecture, each REMA is solely connected to a single RF chain. This configuration is referred to as the PC-REMAA. Due to the connection constraints between the RF chains and antennas, only one candidate antenna is activated at a time for each REMA in PC-REMAA. In other words, each RF chain can select only one antenna from the set of candidate antennas associated with its connected REMA.

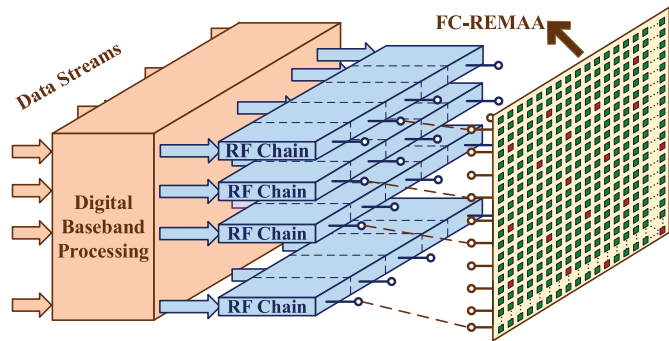


Fig. 3. Illustration of the signal processing architecture for the FC-REMAA.

To enhance the design flexibility of the PC-REMAA, a configuration called the FC-REMAA is further proposed, as illustrated in Fig. 3. In this architecture, the entire antenna array is implemented using an RPA. By dynamically controlling the states of RF switches between pixels, multiple candidate antennas are selected at a time and then connected to the RF chains. In the FC-REMAA, each RF chain has the capability to connect to any of the selected candidate antennas. To facilitate this flexibility, an additional switch network is required to manage the connections between the RF chains and the dynamically selected antennas.

Remark 2: The comparison between PC-REMAA and FC-REMAA demonstrates distinct trade-offs in hardware complexity, power efficiency, and system performance. PC-REMAA offers simpler deployment and lower power consumption but is limited in flexibility and performance. In contrast, FC-REMAA provides better performance and greater flexibility at the cost of higher design complexity and power consumption. Specifically, FC-REMAA requires simultaneous activation of multiple candidate antennas, which demands careful antenna design to manage mutual coupling and maintain impedance matching. The addition of a switch network to enable flexible connections between RF chains and candidate antennas further increases complexity, insertion loss, and power consumption [37]. Additionally, the scalability of FC-REMAA is challenged by the quadratic growth of switch network complexity as the number of antennas and RF chains increases. PC-REMAA simplifies hardware implementation by connecting one REMA to an RF chain. The fixed one-to-one mapping reduces circuit complexity, insertion loss, and power consumption. However, this limits flexibility, as each RF chain can only access one candidate antenna per REMA, reducing spatial diversity and beamforming capabilities compared to FC-REMAA, particularly in complex beamforming or rapid spatial adaptation scenarios. These trade-offs suggest that PC-REMAA is suitable for cost-sensitive deployments with moderate performance needs, while FC-REMAA is better suited for high-performance systems requiring flexibility and capacity optimization.

III. SYSTEM MODEL AND PROBLEM FORMULATION

A. System Model

As illustrated in Fig. 4, we consider a multiuser communication system, where a BS employs a PC-REMAA or an

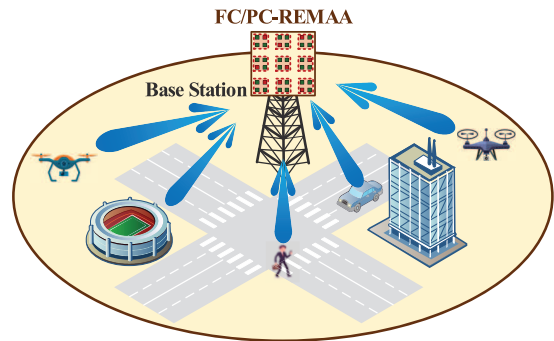


Fig. 4. Illustration of the multiuser communication system with REMAAs.

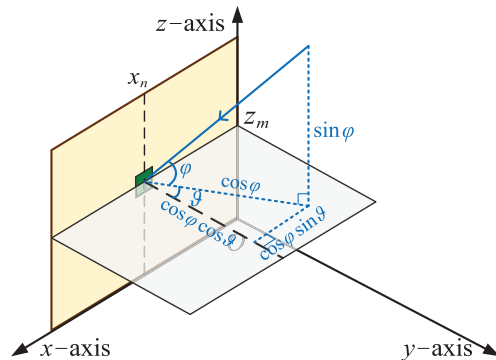


Fig. 5. Illustration of the channel spatial angles in cartesian coordinate system.

FC-REMAA to serve K single-antenna users. Without loss of generality, we assume the antennas of both the PC-REMAA and FC-REMAA are arranged in a uniform planar array. If the PC-REMAA is employed, the transmit array includes M_r rows and M_c columns of REMAs. From Section II-A, by controlling the connections between pixels, each REMA can adjust the radiation pattern to change the radiation position for signal transmission and thus form a series of candidate antennas. Suppose each REMA can support S_r rows and S_c columns of candidate antennas. As a result, the total candidate antennas in each row and column of the PC-REMAA are $N_c = M_c S_c$ and $N_r = M_r S_r$, respectively. Then, the total number of candidate antennas in the PC-REMAA is $N_t = N_r N_c$. On the other hand, if the FC-REMAA is employed, the whole antenna array can be taken as a large-scale RPA. We assume candidate antennas in each row and each column of the FC-REMAA are the same as those of the PC-REMAA for simplicity. Then, the whole FC-REMAA also includes $N_t = N_r N_c$ candidate antennas in total. The spacing between adjacent candidate antennas for both the PC-REMAA and the FC-REMAA is denoted as d_c while the spacing between adjacent REMAs for the PC-REMAA is denoted as d_e . In this work, we focus on the design of the REMAs at the BS and the antenna positions at the users are assumed to be fixed.

For REMA-based multiuser communications, the channels between the BS and the users are determined by propagation environments and the positions of candidate antennas. To represent the positions of candidate antennas, in Fig. 5, we establish a Cartesian coordinate system with the antenna

located at the N_r th row and the N_c th column as the origin. Denote the coordinate of the candidate antenna located at the m th row and the n th column as $[x_n, 0, z_m]$. The steering vector for the channel path with azimuth angle ϑ and elevation angle φ can be expressed as

$$\boldsymbol{\alpha}(N_t, \vartheta, \varphi) = \sqrt{\frac{1}{N_t}} e^{j2\pi \mathbf{x} \cos \varphi \sin \vartheta / \lambda} \otimes e^{j2\pi \mathbf{z} \sin \varphi / \lambda}, \quad (1)$$

where λ denotes the carrier wavelength, $\mathbf{x} \triangleq [x_1, x_2, \dots, x_{N_c}]^T$, and $\mathbf{z} \triangleq [z_1, z_2, \dots, z_{N_r}]^T$. Then, the channel between the BS and the k th user can be expressed as

$$\mathbf{h}_k = \sum_{l=1}^{L_k} \gamma_k^{(l)} \boldsymbol{\alpha}(N_t, \theta_k^{(l)}, \phi_k^{(l)}), \quad (2)$$

where L_k denotes the number of channel paths, $\gamma_k^{(l)}$, $\theta_k^{(l)}$ and $\phi_k^{(l)}$ denote the channel gain, the azimuth angle and the elevation angle of the l th path, respectively. For the PC-REMAA, x_n and z_m can be expressed as

$$\begin{aligned} x_n &= (M_c - q)d_e + (S_c - t)d_c, \\ z_m &= (M_r - p)d_e + (S_r - s)d_c, \end{aligned} \quad (3)$$

where we assume that the antenna, located at the s th row and t th column of the REMA in the p th row and q th column, corresponds to the antenna at the m th row and n th column of the PC-REMAA, i.e., $m = (p-1)S_r + s$ and $n = (q-1)S_c + t$. According to the PC-REMAA settings, we have $p \in \{1, 2, \dots, M_r\}$, $q \in \{1, 2, \dots, M_c\}$, $s \in \{1, 2, \dots, S_r\}$, and $t \in \{1, 2, \dots, S_c\}$. For the FC-REMAA, x_n and z_m can be expressed as

$$x_n = (N_c - n)d_c, \text{ and } z_m = (N_r - m)d_c. \quad (4)$$

Substituting x_n and z_m from (3) and (4) into (2), we can obtain the channels for the PC-REMAA and FC-REMAA, respectively.

B. Problem Formulation

Due to the interference among signals from different channel paths, both the signal strengths and phases vary across the candidate antennas of the PC/FC-REMAA. Usually, greater signal strength corresponds to a higher received signal-to-noise ratio (SNR) and thus leads to better communication quality, which indicates that selecting antennas with stronger signals results in better communication performance. In addition, due to variations in channel state information, the optimal antenna configuration may also change over time. Thus, dynamic antenna selection is required to adapt to these varying channel conditions and optimize communication performance. Denote the number of selected antennas and RF chains as N_s and N_{RF} , respectively. To perform baseband processing, each of the selected antennas is solely connected to an RF chain. Then, we have $N_s \leq N_{\text{RF}}$, limited by the number of RF chains. In addition, the number of selected antennas must exceed the number of users to support independent transmission, i.e., $N_s \geq K$.

Denote the selection matrix as $\mathbf{T} \in \mathbb{Z}^{N_r \times N_c}$, where each entry is one or zero, i.e.,

$$[\mathbf{T}]_{m,n} \in \{0, 1\}. \quad (5)$$

If $[\mathbf{T}]_{m,n}$ is one, the candidate antenna located at the m th row and n th column is selected for data transmission; otherwise, it is not selected. Since N_s antennas are selected, we have

$$\sum_{m=1}^{N_r} \sum_{n=1}^{N_c} [\mathbf{T}]_{m,n} = N_s. \quad (6)$$

To avoid coupling effects between selected antennas, the minimum row and column spacings between selected antennas usually exceed $\lambda/2$, which can be easily converted to the minimum antenna index spacing D by considering the configurations of PC/FC-REMAA. For example, we have $D = \lceil \lambda / (2d_c) \rceil$ for the FC-REMAA. If an antenna located at the m th row and n th column is selected, then antennas within a square region centered at the selected antenna extending D rows and columns in both directions, cannot be selected. This restriction can be mathematically formulated as

$$\sum_{a=m-D}^{m+D} \sum_{b=n-D}^{n+D} [\mathbf{T}]_{a,b} \leq 1, \quad (7)$$

for $m = D+1, \dots, N_r - D$ and $n = D+1, \dots, N_c - D$. The constraint in (7) can be equivalently expressed in matrix form as

$$\sum_{a=1}^{N_r} \sum_{b=1}^{N_c} [\mathbf{B}_{m,n}]_{a,b} [\mathbf{T}]_{a,b} \leq 1, \quad (8)$$

where $\mathbf{B}_{m,n} \in \mathbb{Z}^{N_r \times N_c}$ is defined as

$$[\mathbf{B}_{m,n}]_{a,b} = \begin{cases} 1, & a \in [m-D, m+D], \text{ and } b \in [n-D, n+D], \\ 0, & \text{others.} \end{cases} \quad (9)$$

Note that $\mathbf{B}_{m,n}$ characterizes the selection constraints by marking positions within the exclusion zone with ones, while positions outside this region remain zero.

For the PC-REMAA, only one antenna can be selected from the candidate antennas within each REMA, as these candidate antennas are exclusively connected to a single RF chain. This constraint can be expressed as

$$\sum_{m=(p-1)S_r+1}^{pS_r} \sum_{n=(q-1)S_c+1}^{qS_c} [\mathbf{T}]_{m,n} = 1, \quad (10)$$

for $p = 1, \dots, M_r$ and $q = 1, \dots, M_c$. Similar to (8), (10) can also be equivalently rewritten as

$$\sum_{a=1}^{N_r} \sum_{b=1}^{N_c} [\mathbf{C}_{p,q}]_{a,b} [\mathbf{T}]_{a,b} = 1, \quad (11)$$

where $\mathbf{C}_{p,q} \in \mathbb{Z}^{N_r \times N_c}$ is defined as

$$[\mathbf{C}_{p,q}]_{a,b} = \begin{cases} 1, & a \in [(p-1)S_r + 1, pS_r] \\ & b \in [(q-1)S_c + 1, qS_c], \\ 0, & \text{others.} \end{cases} \quad (12)$$

Here, $\mathbf{C}_{p,q}$ characterizes the selection constraints for the PC-REMAA by marking the positions of candidate antennas

within the REMA located at the p th row and q th column with ones, while all other positions remain zero.

To facilitate following formulations, we vectorize the selection matrix \mathbf{T} as $\mathbf{t} \triangleq \text{vec}\{\mathbf{T}\}$. Then the constraints in (5), (6), (7), and (10) can be respectively expressed as

$$[\mathbf{t}]_p \in \{0, 1\}, \text{ for } p = 1, 2, \dots, N_t, \quad (13a)$$

$$\mathbf{1}_{N_t}^T \mathbf{t} = N_s, \quad (13b)$$

$$\mathbf{S}^T \mathbf{t} \leq \mathbf{1}_{N_t}, \quad (13c)$$

$$\mathbf{Q}^T \mathbf{t} = \mathbf{1}_{M_t}. \quad (13d)$$

In (13c), $\mathbf{S} \in \mathbb{Z}^{N_t \times N_t}$ denotes the spacing constraint matrix and can be expressed as

$$[\mathbf{S}]_{:,s} = \text{vec}\{\mathbf{B}_{m,n}\}, \quad (14)$$

for $s = (n-1)N_r + m$, $m = 1, \dots, N_r$, and $n = 1, \dots, N_c$. In (13d), $M_t \triangleq M_r M_c$ denotes the number of REMAs in the PC-REMAA. $\mathbf{Q} \in \mathbb{Z}^{N_t \times M_t}$ denotes the partially-connected antenna selection constraint matrix and can be expressed as

$$[\mathbf{Q}]_{:,s} = \text{vec}\{\mathbf{C}_{p,q}\}, \quad (15)$$

for $s = (q-1)M_r + p$, $p = 1, \dots, M_r$, and $q = 1, \dots, M_c$. Then, we respectively denote the sets of \mathbf{t} for the PC-REMAA and FC-REMAA as

$$\begin{aligned} \Phi_P &= \{\mathbf{t} \in \mathbb{Z}^{N_t} \mid (13a), (13b), (13c), \text{ and } (13d)\}, \\ \Phi_F &= \{\mathbf{t} \in \mathbb{Z}^{N_t} \mid (13a), (13b), \text{ and } (13c)\}. \end{aligned} \quad (16)$$

In this work, we aim at maximizing the sum-rate of K users by selecting N_s antennas from the N_t candidate antennas and optimizing the multiuser beamforming, subject to the constraints in (5), (6), (7), and (10). The optimization problem can be formulated as

$$\max_{\mathbf{F}, \mathbf{t}} \sum_{k=1}^K R_k \quad (17a)$$

$$\text{s.t. } \|\mathbf{F}\|_F^2 \leq P, \quad (17b)$$

$$\mathbf{t} \in \Phi_P \text{ or } \Phi_F. \quad (17c)$$

In (17a), R_k represents the achievable data rate of the k th user and is given by

$$R_k = \log_2 \left(1 + \frac{|\mathbf{h}_k^H \bar{\mathbf{T}} \mathbf{f}_k|^2}{\sigma^2 + \sum_{i=1, i \neq k}^K |\mathbf{h}_k^H \bar{\mathbf{T}} \mathbf{f}_i|^2} \right), \quad (18)$$

where $\bar{\mathbf{T}} \triangleq \text{diag}\{\mathbf{t}\}$, $\mathbf{f}_k \triangleq [\mathbf{F}]_{:,k}$, and $\mathbf{F} \in \mathbb{C}^{N_t \times K}$ denotes the multiuser transmit beamforming matrix. Constraint in (17b) ensures that the total transmit power satisfies the power budget, i.e., $\|\mathbf{F}\|_F^2 \leq P$, where P represents the maximum allowable transmit power. In (17c), \mathbf{t} belongs to different feasible sets depending on the employed REMAA architecture: $\mathbf{t} \in \Phi_P$ for PC-REMAA and $\mathbf{t} \in \Phi_F$ for FC-REMAA.

Remark 3: Note that the channel state information between the PC/FC-REMAA and users can be obtained via channel estimation techniques in [38], [39], and [40]. In this work, we focus on the multiuser beamforming and assume that the channel state information is known in advance.

Remark 4: In this work, we assume the PC-REMAA and FC-REMAA are arranged in a uniform planar array to simplify

the analysis. In practice, the array configurations may not be uniform and planar. We then discuss the extensions of the proposed methods. From Section III, two components including the channels in the system model and the constraints in the problem formulation are influenced by the antenna configurations. From (1), the channels between the BS and the users are determined by the antenna positions. Therefore, once the antenna positions are obtained, the channel models can be readily determined. From (13), four constraints are included for the candidate antenna selection. The first two constraints are the same for all array configurations. The spacing constraint in (13c) and exclusive constraint in (13d) can be obtained based on the specific geometry of the array. Once the channels and constraints are specified, the sum-rate maximization problem can be established for arbitrary array configurations. Therefore, the proposed methods can also be extended to other array configurations.

IV. MULTIUSER BEAMFORMING AND ANTENNA SELECTION FOR REMAAS

In this section, we focus on solving (17) for the design of multiuser beamforming and antenna selection in PC/FC-REMAA, where a TS-MBAS scheme is proposed. In the first step of the TS-MBAS scheme, we propose a TL-JBAS algorithm, as elaborated from Section IV-A to Section IV-D. In the second step of the TS-MBAS scheme, we apply the coordinate descent method to further enhance the solution of the TL-JBAS algorithm, as presented in Section IV-E.

A. Problem Conversion

Note that (17) involves a nonconvex objective function, as shown in (17a), and binary constraints, as defined in (5), which makes the problem a mixed-integer nonlinear programming (MINLP) problem. According to [41], MINLP problems are widely recognized as nondeterministic polynomial-time hard and it is unlikely to achieve optimality in polynomial time. Therefore, we turn to convert (17) into a tractable form to efficiently find a suboptimal solution.

First, we focus on the power constraint in (17b). Based on Proposition 3 in [42], any nontrivial stationary point of the beamforming matrix \mathbf{F} that maximizes the sum-rate will satisfy the power constraint with equality. This property allows us to simplify the problem by removing the power constraint from (17b). As a result, we can reformulate (17) into a more tractable and equivalent form as

$$\max_{\mathbf{F}, \mathbf{t}} \sum_{k=1}^K \tilde{R}_k \quad (19a)$$

$$\text{s.t. } \mathbf{t} \in \Phi_P \text{ or } \Phi_F, \quad (19b)$$

where \tilde{R}_k can be expressed as

$$\tilde{R}_k = \log_2 \left(1 + \frac{|\mathbf{h}_k^H \bar{\mathbf{T}} \mathbf{f}_k|^2}{\frac{\sigma^2 \|\mathbf{F}\|_F^2}{P} + \sum_{i=1, i \neq k}^K |\mathbf{h}_k^H \bar{\mathbf{T}} \mathbf{f}_i|^2} \right). \quad (20)$$

Then, we turn our attention to the nonconvex objective in (19a). By applying Lemma 4.1 from [43], we can address the

objective function in (19a) and convert (19) into an equivalent form as

$$\min_{u_k, v_k, \mathbf{F}, \mathbf{t}} \sum_{k=1}^K v_k e_k - \log v_k \quad (21a)$$

$$\text{s.t. } \mathbf{t} \in \Phi_P \text{ or } \Phi_F, \quad (21b)$$

where e_k is defined as

$$e_k = \sum_{i=1, i \neq k}^K |u_k \mathbf{h}_k^H \bar{\mathbf{T}} \mathbf{f}_i|^2 + |u_k \mathbf{h}_k^H \bar{\mathbf{T}} \mathbf{f}_k - 1|^2 + \frac{|u_k|^2 \sigma^2 \|\mathbf{F}\|_F^2}{P}, \quad (22)$$

and u_k is the receive factor of the k th user.

Furthermore, we consider the antenna selection constraint in (21b). Note that (21) adapts to both the PC-REMAA and FC-REMAA by adjusting the constraint in (21b). From (16), the PC-REMAA includes an additional constraint in (13d), which makes its design more complex compared to the FC-REMAA. Due to this added difficulty, we focus on solving (21) for the PC-REMAA in this work. Once the algorithm is developed, it can be directly applied to the FC-REMAA by simply removing the additional constraint in (13d).

To handle the binary constraint in Φ_P , we use the equivalent continuous formulation from [44], expressed as

$$[\mathbf{t}]_p(1 - [\mathbf{t}]_p) = 0, \text{ for } p = 1, 2, \dots, N_t. \quad (23)$$

Using this, the feasible set Φ_P can be rewritten as

$$\Phi_P = \{\mathbf{t} \in \mathbb{Z}^{N_t} \mid (23), (13b), (13c), \text{ and } (13d)\}. \quad (24)$$

Note that Φ_P in (24) contains three equality constraints and one inequality constraint. The presence of multiple equality constraints reduces the degrees of freedom in the optimization, which may lead to lower-quality solutions. To address this issue, we employ the penalty-based method to relax the equality constraints and incorporate them into the objective. This reformulation transforms (21) into the following problem:

$$\min_{u_k, v_k, \mathbf{F}, \mathbf{t}} \mathcal{L}(u_k, v_k, \mathbf{F}, \mathbf{t}) \quad (25a)$$

$$\text{s.t. } \mathbf{S}^T \mathbf{t} \leq \mathbf{1}_{N_t}, \quad (25b)$$

$$[\mathbf{t}]_p \in [0, 1], \text{ for } p = 1, 2, \dots, N_t. \quad (25c)$$

In (25a), $\mathcal{L}(u_k, v_k, \mathbf{F}, \mathbf{t})$ represents a weighted sum of the original objective function and the penalty terms for the relaxed constraints, given by

$$\begin{aligned} \mathcal{L}(u_k, v_k, \mathbf{F}, \mathbf{t}) \triangleq & \sum_{k=1}^K (v_k e_k - \log v_k) + \rho_1 \mathbf{t}^T (\mathbf{1}_{N_t} - \mathbf{t}) \\ & + \rho_2 \|\mathbf{1}_{N_t}^T \mathbf{t} - N_s\|_2^2 + \rho_3 \|\mathbf{Q}^T \mathbf{t} - \mathbf{1}_{M_t}\|_2^2, \end{aligned} \quad (26)$$

where $\rho_1 > 0$, $\rho_2 > 0$, and $\rho_3 > 0$ are penalty coefficients that control the relaxation of the constraints. In this new formulation, the inequality constraint in (25b) is retained, while an additional box constraint in (25c) is introduced to further refine the feasible region. With this reformulation in place, we now proceed to develop the TL-JBAS algorithm to efficiently solve (25).

B. Description of the TL-JBAS Algorithm

The TL-JBAS algorithm follows a two-loop iterative framework to optimize beamforming and antenna selection efficiently.

In the outer loop, the penalty coefficients ρ_1 , ρ_2 , and ρ_3 are initially set to 1 to provide a well-conditioned starting point. These coefficients are then gradually increased by multiplying them with scaling factors β_1 , β_2 , and β_3 , each of which is greater than 1. This gradual adjustment ensures that the equality constraints are eventually satisfied while maintaining numerical stability.

In the inner loop, the penalty coefficients remain fixed, and an alternating minimization method is employed to iteratively optimize u_k , v_k , \mathbf{F} , and \mathbf{t} .

C. Description of the Alternating Minimization Method

1) *Initialization*: First, the alternating minimization method is initialized by assuming that all antennas are selected. Accordingly, the antenna selection vector \mathbf{t} is set as

$$\mathbf{t} = \mathbf{1}_{N_t}. \quad (27)$$

Next, to maximize the received power for each user at the start, the beamforming matrix \mathbf{F} is initialized based on the channel state information, given by

$$\mathbf{F} = \mathbf{H}. \quad (28)$$

2) *Optimization of u_k* : When optimizing u_k while keeping other variables fixed, the problem in (21) simplifies to

$$\min_{u_k} e_k. \quad (29)$$

Next, we first compute the partial derivative of e_k with respect to u_k^* , given by

$$\frac{\partial e_k}{\partial u_k^*} = \left(\sum_{i=1}^K |\mathbf{h}_k^H \bar{\mathbf{T}} \mathbf{f}_i|^2 + \frac{\sigma^2 \|\mathbf{F}\|_F^2}{P} \right) u_k - \mathbf{f}_k^H \bar{\mathbf{T}} \mathbf{h}_k. \quad (30)$$

Setting the derivative to zero, i.e., $\partial e_k / \partial u_k^* = 0$, we obtain the optimal solution for (29) as

$$\tilde{u}_k = \frac{\mathbf{f}_k^H \bar{\mathbf{T}} \mathbf{h}_k}{\sum_{i=1}^K |\mathbf{h}_k^H \bar{\mathbf{T}} \mathbf{f}_i|^2 + \frac{\sigma^2 \|\mathbf{F}\|_F^2}{P}}. \quad (31)$$

3) *Optimization of v_k* : When optimizing v_k while keeping other variables fixed, the problem in (21) reduces to

$$\min_{v_k} v_k e_k - \log v_k. \quad (32)$$

To determine the optimal solution, we apply the first-order optimality condition by differentiating the objective function with respect to v_k and setting it to zero. Solving for v_k , we obtain

$$\tilde{v}_k = \frac{1}{e_k}. \quad (33)$$

4) *Optimization of \mathbf{f}_k* : When optimizing \mathbf{f}_k while keeping other variables fixed, the problem in (21) reduces to

$$\min_{\mathbf{f}_k} \sum_{k=1}^K v_k e_k. \quad (34)$$

Next, we compute the gradient of the objective function with respect to \mathbf{f}_k^* , yielding

$$\sum_{i=1}^K v_i \frac{\partial e_i}{\partial \mathbf{f}_k^*} = \Psi \mathbf{f}_k - \eta, \quad (35)$$

where the terms Ψ and η are defined as

$$\begin{aligned} \Psi &= \sum_{i=1}^K v_i |u_i|^2 \left(\bar{\mathbf{T}} \mathbf{h}_i \mathbf{h}_i^H \bar{\mathbf{T}}^T + \frac{\sigma^2}{P} \mathbf{I}_{N_t} \right), \\ \eta &= v_k u_k^* \bar{\mathbf{T}} \mathbf{h}_k. \end{aligned} \quad (36)$$

By setting $\sum_{i=1}^K v_i \frac{\partial e_i}{\partial \mathbf{f}_k^*} = \mathbf{0}$, we obtain the optimal solution for (34) as

$$\tilde{\mathbf{f}}_k = \Psi^{-1} \eta. \quad (37)$$

By stacking $\tilde{\mathbf{f}}_k$ for all users, we obtain the optimized beamforming matrix $\tilde{\mathbf{F}}$.

5) *Optimization of \mathbf{t}* : In this part, we optimize \mathbf{t} while keeping other variables fixed. The objective function can be expressed as

$$\begin{aligned} \mathcal{L}(u_k, v_k, \mathbf{F}, \mathbf{t}) &\propto \sum_{k=1}^K v_k e_k + \rho_1 \mathbf{t}^T (\mathbf{1}_{N_t} - \mathbf{t}) \\ &\quad + \rho_2 \|\mathbf{1}_{N_t}^T \mathbf{t} - N_s\|_2^2 + \rho_3 \|\mathbf{Q}^T \mathbf{t} - \mathbf{1}_{M_t}\|_2^2. \end{aligned}$$

where \propto denotes ‘‘proportional to’’ indicating that terms independent of the optimization variables are omitted. Expanding e_k , we rewrite the above function as

$$\begin{aligned} \mathcal{L}(u_k, v_k, \mathbf{F}, \mathbf{t}) &\propto \sum_{k=1}^K v_k \left(\sum_{i=1}^K |u_k \mathbf{h}_k^H \bar{\mathbf{T}} \mathbf{f}_i|^2 - 2\mathcal{R}\{u_k \mathbf{h}_k^H \bar{\mathbf{T}} \mathbf{f}_k\} \right) \\ &\quad - \rho_1 (\mathbf{t}^T \mathbf{t} - \mathbf{1}_{N_t}^T \mathbf{t}) + \rho_2 (\mathbf{t}^T \mathbf{1}_{N_t} \mathbf{1}_{N_t}^T \mathbf{t} - 2N_s \mathbf{1}_{N_t}^T \mathbf{t}) \\ &\quad + \rho_3 \mathbf{t}^T \mathbf{Q} \mathbf{Q}^T \mathbf{t} - 2\mathbf{1}_{M_t}^T \mathbf{Q}^T \mathbf{t}. \end{aligned} \quad (38)$$

To facilitate further analysis, we define $\mathbf{w}_{k,i} \triangleq \mathbf{h}_k^* \odot \mathbf{f}_i$ and rewrite the objective as

$$\begin{aligned} \mathcal{L}(u_k, v_k, \mathbf{F}, \mathbf{t}) &= \sum_{k=1}^K v_k \left(\sum_{i=1}^K |u_k \mathbf{t}^T \mathbf{w}_{k,i}|^2 - 2\mathcal{R}\{u_k \mathbf{t}^T \mathbf{w}_{k,k}\} \right) \\ &\quad + \mathbf{t}^T (-\rho_1 \mathbf{I}_{N_t} + \rho_2 \mathbf{1}_{N_t} \mathbf{1}_{N_t}^T + \rho_3 \mathbf{Q} \mathbf{Q}^T) \mathbf{t} \\ &\quad + (\rho_1 \mathbf{1}_{N_t}^T - 2\rho_2 N_s \mathbf{1}_{N_t}^T - 2\mathbf{1}_{M_t}^T \mathbf{Q}^T) \mathbf{t} \\ &\stackrel{(a)}{=} \mathbf{t}^T \mathbf{U} \mathbf{t} + \mathbf{u}^T \mathbf{t}, \end{aligned} \quad (39)$$

where in (a), we define

$$\mathbf{U} \triangleq \sum_{k=1}^K v_k |u_k|^2 \sum_{i=1}^K \mathbf{w}_{k,i} \mathbf{w}_{k,i}^H - \rho_1 \mathbf{I}_{N_t} + \rho_2 \mathbf{1}_{N_t} \mathbf{1}_{N_t}^T + \rho_3 \mathbf{Q} \mathbf{Q}^T$$

$$\mathbf{u} \triangleq -2 \sum_{k=1}^K v_k \mathcal{R}\{u_k \mathbf{w}_{k,k}\} + \rho_1 \mathbf{1}_{N_t} - 2\rho_2 N_s \mathbf{1}_{N_t} - 2\mathbf{Q} \mathbf{1}_{M_t}. \quad (40)$$

Thus, the optimization problem reduces to

$$\min_{\mathbf{t}} \mathbf{t}^T \mathbf{U} \mathbf{t} + \mathbf{u}^T \mathbf{t}, \quad (41a)$$

$$\text{s.t. } \mathbf{S}^T \mathbf{t} \leq \mathbf{1}_{N_t}, \quad (41b)$$

$$[\mathbf{t}]_p \in [0, 1], \quad \forall p = 1, 2, \dots, N_t. \quad (41c)$$

Since \mathbf{U} contains the term $-\rho_1 \mathbf{I}_{N_t}$ in (40), it may not necessarily be positive definite.

- If \mathbf{U} is positive definite, (41) becomes a convex quadratic program and can be efficiently solved using CVX.
- If \mathbf{U} is not positive definite, (41) is nonconvex, requiring more sophisticated optimization methods such as the interior-point method. These methods are well established and can be implemented using standard optimization toolboxes. For further details, we refer the interested reader to [45].

By solving (41), we obtain the antenna selection vector $\tilde{\mathbf{t}}$.

6) *Stop Conditions*: We repeat the procedures from Section IV-C2 to Section IV-C5 to alternately optimize u_k , v_k , \mathbf{F} , and \mathbf{t} until the maximum number of iterations is reached or the alternating minimization method converges.

D. Stopping Conditions of the TL-JBAS Algorithm

To determine whether an antenna is selected, we introduce a threshold \mathcal{Y} . Specifically, if $[\tilde{\mathbf{t}}]_n \geq \mathcal{Y}$, the n th antenna is selected; otherwise, it is not included in the final selection.

We iteratively update the penalty parameters ρ_1 , ρ_2 , and ρ_3 in the outer loop and perform the alternating minimization method in the inner loop, until the number of selected antennas equals N_s and the variations of the optimization variables fall below a predefined threshold. The final selection vector is

$$[\hat{\mathbf{t}}]_n = \begin{cases} 1, & [\tilde{\mathbf{t}}]_n \geq \mathcal{Y}, \\ 0, & \text{otherwise.} \end{cases} \quad (42)$$

Substituting $\hat{\mathbf{t}}$ into the original problem in (17), we reformulate the optimization problem as

$$\begin{aligned} \max_{\mathbf{F}} \quad & \sum_{k=1}^K \log_2 \left(1 + \frac{|\mathbf{h}_k^H \text{diag}(\hat{\mathbf{t}}) \mathbf{f}_k|^2}{\sigma^2 + \sum_{i=1, i \neq k}^K |\mathbf{h}_k^H \text{diag}(\hat{\mathbf{t}}) \mathbf{f}_i|^2} \right) \\ \text{s.t.} \quad & \|\mathbf{F}\|_F^2 \leq P. \end{aligned} \quad (43)$$

The optimization problem in (43) is a multiuser sum-rate maximization problem, which can be effectively solved using the weighted minimum mean squared error (WMMSE) framework [42], [43]. As WMMSE-based solutions are well-established, we omit the detailed derivation and denote the resulting maximized sum-rate as V .

E. Enhancement With the Coordinate Descent Method

In this part, we present the second step of the TS-MBAS scheme, where the coordinate descent method is employed to enhance the performance of the TL-JBAS algorithm. The

core idea is to iteratively evaluate the selected antennas by sequentially swapping each selected antenna with a candidate antenna. Specifically, when each selected antenna is replaced by a candidate antenna, a multiuser sum-rate maximization problem is solved and the maximized sum-rate is calculated. If the replacement improves the sum-rate, the swap is accepted; otherwise, the original selection is retained. This process continues until no further sum-rate improvement can be achieved through any single swap.

According to Section IV-D, the TL-JBAS algorithm selects N_s antennas. We denote the index of the n th selected antenna as I_n , for $n = 1, 2, \dots, N_s$. Then we denote the initial antenna selection vector as $\bar{\mathbf{t}}_0 \leftarrow \bar{\mathbf{t}}$ and iteratively evaluate the selected antennas.

1) *Iterative Antenna Swapping*: In the d th iteration, for $d \geq 1$, we initialize the antenna selection vector as $\bar{\mathbf{t}}_d \leftarrow \bar{\mathbf{t}}_{d-1}$. The index of the antenna under evaluation is given by

$$n = \text{mod}(d - 1, N_s) + 1. \quad (44)$$

Next, we deactivate the I_n th antenna by setting

$$[\bar{\mathbf{t}}_d]_{I_n} = 0. \quad (45)$$

We then sequentially evaluate all N_t candidate antennas. When evaluating the p th candidate antenna, for $p = 1, 2, \dots, N_t$, the updated selection vector is given by

$$[\bar{\mathbf{t}}_d]_p \leftarrow 1. \quad (46)$$

2) *Sum-Rate Evaluation*: For each selection vector $\bar{\mathbf{t}}_d$, we verify whether it belongs to the feasible set Φ_P or Φ_F . If so, we substitute $\hat{\mathbf{t}}$ in (43) with $\bar{\mathbf{t}}_d$ and solve it using the WMMSE approach. The resulting sum-rate for this evaluation is denoted as \bar{V}_p . If the selection is infeasible, we set $\bar{V}_p \leftarrow 0$.

The index of the antenna yielding the maximum sum-rate for the evaluation of the n th antenna in the d th iteration is determined as

$$\bar{p}_d^{(n)} = \arg \max_{p=1,2,\dots,N_t} \bar{V}_p. \quad (47)$$

The corresponding sum-rate for the d th iteration is denoted as \hat{V}_d . The index of the n th selected antennas, I_n , is then updated as

$$I_n \leftarrow \bar{p}_d^{(n)}. \quad (48)$$

3) *Stop Conditions*: The iterative process continues following the steps from (44) to (48) until the stopping condition

$$\bar{p}_d^{(n)} = \bar{p}_{d-N_s}^{(n)}, \quad d > N_s, \quad n = 1, 2, \dots, N_s, \quad (49)$$

is satisfied. This condition implies that the selected antennas remain unchanged compared to those chosen N_s iterations earlier, indicating that no further improvement can be achieved through any single swap.

4) *Final Optimization Outcome*: Upon convergence, the optimized sum-rate after enhancement is obtained as

$$\tilde{V} \leftarrow \hat{V}_d, \quad (50)$$

which completes the enhancement procedures.

Finally, we summarize the TS-MBAS scheme, including the TL-JBAS algorithm in the first step and the enhancement

Algorithm 1 Two-Step Multiuser Beamforming and Antenna Selection (TS-MBAS) Scheme

```

1 Input:  $N_r, N_c, N_t, S_r, S_c, Q_r, Q_c, P, K, \Upsilon$ , and  $\mathbf{h}_k$ .
2 Initialization:  $\rho_1 \leftarrow 1, \rho_2 \leftarrow 1$ , and  $\rho_3 \leftarrow 1$ .
3 /*Step 1: The TL-JBAS Algorithm*/
4 while conditions in Sec. IV-D are not satisfied do
5    $\rho_1 \leftarrow \rho_1 \beta_1, \rho_2 \leftarrow \rho_2 \beta_2$ , and  $\rho_3 \leftarrow \rho_3 \beta_3$ .
6   /*The Alternating Minimization Method*/
7   while conditions in Sec. IV-C.6 are not satisfied do
8     Initialize  $\mathbf{t}$  and  $\mathbf{F}$  via (27) and (28), respectively.
9     Obtain  $\tilde{u}_k$  via (31).
10    Obtain  $\tilde{v}_k$  via (33).
11    Obtain  $\tilde{f}_k$  via (37).
12    Obtain  $\mathbf{t}$  via (41).
13  end while
14 end while
15 Obtain  $\hat{\mathbf{t}}$  via (42).
16 /*Step 2: Enhancement*/
17  $\bar{\mathbf{t}}_0 \leftarrow \hat{\mathbf{t}}$  and  $d \leftarrow 0$ .
18 while conditions in (49) are not satisfied do
19    $d \leftarrow d + 1$ .
20   Obtain  $n$  via (44).
21   Obtain  $\bar{p}_d^{(n)}$  via (47).
22   Obtain  $\hat{V}_d$  by solving (43).
23 end while
24  $\tilde{V} \leftarrow \hat{V}_d$ .
25 Output:  $\tilde{V}$ .

```

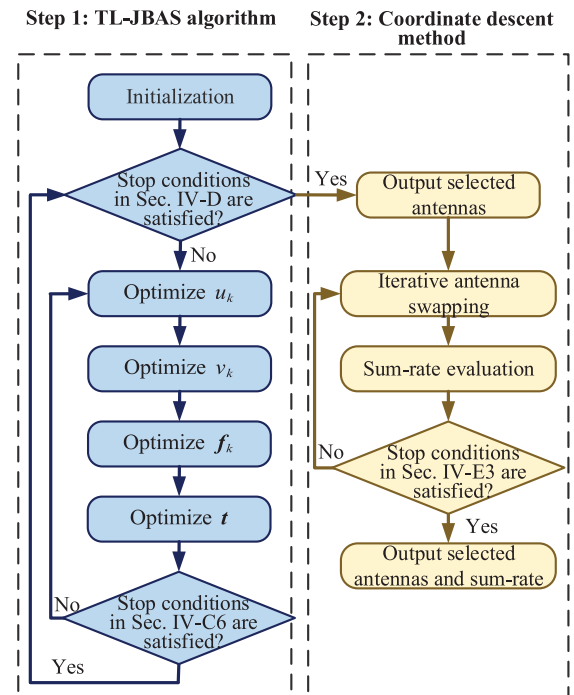


Fig. 6. Illustration of the flow chart of the TS-MBAS scheme.

using the coordinate descent method in the second step, in **Algorithm 1**.

For a clear understanding of the TS-MBAS scheme, we include a flow chart in Fig. 6 to show its key procedures.

In this scheme, the TL-JBAS algorithm is performed in the first step and the coordinate descent method is performed in the second step. The TL-JBAS algorithm includes two loops, where the penalty coefficients including ρ_1 , ρ_2 , and ρ_3 are increased in the outer loop and variables including u_k , v_k , \mathbf{F} , and \mathbf{t} are iteratively optimized in the inner loop. When the stop conditions of the outer loop are satisfied, the TL-JBAS algorithm outputs the selected antennas. Then, the coordinate descent method iteratively evaluates the selected antennas by sequentially swapping each selected antenna with a candidate antenna. When the stop conditions of the coordinate descent method are satisfied, the final selected antennas can be determined and the corresponding sum-rate can be obtained.

Now we evaluate the computational complexity of the proposed TS-MBAS scheme. Since the optimizations of u_k , v_k , and \mathbf{F} can be computed in closed form, their computational complexity is negligible. The optimization of \mathbf{t} may involve solving a nonconvex quadratic programming problem. Suppose the interior-point method with A_I iterations is employed. The computational complexity of optimizing \mathbf{t} is $\mathcal{O}(A_I N_t^3)$. Denote the number of loops for the TL-JBAS algorithm as A_L . Then the computational complexity of the TL-JBAS algorithm is $\mathcal{O}(A_L A_I N_t^3)$. In each evaluation of the coordinate descent method, a sum-rate maximization problem in (43) is solved with the WMMSE, which has a computational complexity of $\mathcal{O}(N_s)$ [42]. Suppose the number of iterations for the coordinate descent method is A_C . Each iteration involves fewer than N_t times of evaluation. Then, the computational complexity of the coordinate descent method is $\mathcal{O}(A_C N_t N_s)$. In total, the computational complexity of the TS-MBAS scheme is $\mathcal{O}(A_C N_t N_s + A_L A_I N_t^3)$.

We also discuss the convergence of the proposed TS-MBAS scheme and the optimality of the obtained solution. The TL-JBAS algorithm iteratively optimizes u_k , v_k , \mathbf{F} , and \mathbf{t} to minimize the objective in (25a) in the inner loop. In each optimization step, either a closed-form solution is obtained or an iterative algorithm is employed. Therefore, the objective function is guaranteed to be monotonically non-increasing in the inner loop. The TL-JBAS algorithm gradually increases the penalty coefficients in the outer step and the enforcement of equality constraints is progressively strengthened. As a result, the equality constraints can be satisfied eventually and the required antennas can be selected. The coordinate descent method iteratively evaluates the selected antennas by sequentially swapping each selected antenna with a candidate antenna. If the replacement improves the sum-rate, the swap is accepted; otherwise, the original selection is retained. In this way, the sum-rate is guaranteed to be monotonically non-decreasing and the coordinate descent method converges. Note that the coordinate descent method performs iterative searches for each variable in the quantized space. Therefore, its solution is at least a suboptimal solution of the original problem in (17). In summary, the TS-MBAS scheme converges to at least a suboptimal solution.

V. THE MECHANICAL MOVABLE ANTENNAS: A REVISIT

In this section, to establish a benchmark for evaluating REMA-enabled communications, we revisit MMAs with

continuously adjustable positions within the transmission region. We formulate a sum-rate maximization problem for MMA-enabled multiuser communications and propose an ABAPO scheme to solve it.

A. System and Channel Model

For a fair comparison with REMAs, we assume that the number of antennas in the MMA system is N_s . The three-dimensional coordinate of the n th antenna is denoted as $\mathbf{p}_n \in \mathbb{R}^3$, for $n = 1, 2, \dots, N_s$. The transmission region of the MMAs is identical to that of the REMAs and is denoted as \mathcal{C} , indicating that the antenna positions satisfy the constraint $\mathbf{p}_n \in \mathcal{C}$.

From (2), the channel between the k th user and the N_s antennas can be expressed as

$$\mathbf{g}_k(\mathbf{P}) = \sum_{l=1}^{L_k} \gamma_k^{(l)} \boldsymbol{\beta} \left(N_s, \mathbf{P}, \theta_k^{(l)}, \phi_k^{(l)} \right). \quad (51)$$

$\boldsymbol{\beta}(N_s, \mathbf{P}, \theta, \phi)$ denotes the channel steering vector between the k th user and the N_s MAs, and is given by

$$\boldsymbol{\beta}(N_s, \mathbf{P}, \theta, \phi) = \sqrt{\frac{1}{N_s}} e^{j2\pi \mathbf{P} \mathbf{i}}, \quad (52)$$

where $\mathbf{P} \triangleq [\mathbf{p}_1^T, \mathbf{p}_2^T, \dots, \mathbf{p}_{N_s}^T]^T$ is the stacked position matrix for the N_s MMAs and $\mathbf{i} \triangleq [\cos \phi \sin \theta, \cos \phi \cos \theta, \sin \phi]^T$ is the normalized wave vector.

B. Problem Formulation

Each of the N_s antennas is connected to an RF chain. By designing the baseband beamforming vector $\mathbf{w}_k \in \mathbb{C}^{N_s}$ for each user, we can mitigate multiuser interference and optimize the multiuser sum-rate. Additionally, by adjusting the positions of the N_s MMAs via motors or liquid metals, the multiuser channels can be tuned to achieve appropriate coherence, thus facilitating effective beamforming.

We aim at maximizing the multiuser sum-rate by jointly optimizing the positions of the MMAs, \mathbf{p}_n , and the baseband beamforming vectors, \mathbf{w}_k . The optimization problem is formulated as

$$\max_{\mathbf{p}_n, \mathbf{w}_k} \sum_{k=1}^K \bar{R}_k \quad (53a)$$

$$\text{s.t. } \|\mathbf{W}\|_F^2 \leq P, \quad (53b)$$

$$\mathbf{p}_n \in \mathcal{C}, \quad n = 1, 2, \dots, N_s, \quad (53c)$$

$$\|\mathbf{p}_m - \mathbf{p}_n\|_2 \geq \frac{\lambda}{2}, \quad \forall m \neq n. \quad (53d)$$

In (53a), \bar{R}_k represents the achievable sum-rate for the k th user and can be expressed as

$$\bar{R}_k = \log_2 \left(1 + \frac{|\mathbf{g}_k(\mathbf{P})^H \mathbf{w}_k|^2}{\sigma^2 + \sum_{i=1, i \neq k}^K |\mathbf{g}_k(\mathbf{P})^H \mathbf{w}_i|^2} \right). \quad (54)$$

In (53b), $\mathbf{W} \triangleq [\mathbf{w}_1, \dots, \mathbf{w}_K]$ is the stack of beamforming vectors, and its Frobenius norm is constrained by the total transmit power P . In (53c), the position of each antenna \mathbf{p}_n

is restricted to lie within the predefined transmission region \mathcal{C} . In (53d), the spacing between any two antennas is at least $\lambda/2$ to avoid mutual coupling effects.

The optimization problem in (53) involves the optimization of antenna positions \mathbf{p}_n and beamforming vectors \mathbf{w}_k . These two sets of variables exhibit different characteristics and require distinct optimization techniques. Therefore, it is difficult to optimize them simultaneously. To address this, we then propose an ABAPO scheme to efficiently solve (53) by alternately optimizing the multiuser beamforming and the antenna positions.

C. Alternating Beamforming and Antenna Position Optimization Scheme

Given the antenna positions \mathbf{p}_n , the optimization problem in (53) simplifies to

$$\begin{aligned} \max_{\mathbf{w}_k} \quad & \sum_{k=1}^K \bar{R}_k \\ \text{s.t.} \quad & \|\mathbf{W}\|_{\text{F}}^2 \leq P. \end{aligned} \quad (55)$$

This is a classic multiuser sum-rate maximization problem and can be efficiently solved using the WMMSE framework. We omit the details and denote its solution as $\tilde{\mathbf{w}}_k$.

Given the beamforming vectors \mathbf{w}_k , (53) reduces to

$$\begin{aligned} \max_{\mathbf{p}_n} \quad & \sum_{k=1}^K \bar{R}_k \\ \text{s.t.} \quad & \mathbf{p}_n \in \mathcal{C}, \quad n = 1, 2, \dots, N_s, \\ & \|\mathbf{p}_m - \mathbf{p}_n\|_2 \geq \frac{\lambda}{2}, \quad \forall m \neq n. \end{aligned} \quad (56)$$

This problem is nonconvex due to the structure of both the objective and constraints. We then adopt the interior-point method to solve it [45]. First, we rewrite the transmit region constraint $\mathbf{p}_n \in \mathcal{C}$ as $E(\mathbf{p}_n) \leq 0$ by parameterizing \mathcal{C} . Introducing slack variables $c_n \geq 0$ and $g_{m,n} \geq 0$, we reformulate (56) as

$$\begin{aligned} \min_{\mathbf{p}_n} \quad & -\sum_{k=1}^K \bar{R}_k - \mu \sum_{n=1}^{N_s} \ln c_n - \rho \sum_{m=1}^{N_s} \sum_{n=m+1}^{N_s} \ln g_{m,n} \\ \text{s.t.} \quad & E(\mathbf{p}_n) + c_n = 0, \quad n = 1, 2, \dots, N_s, \\ & \frac{\lambda}{2} - \|\mathbf{p}_m - \mathbf{p}_n\|_2 + g_{m,n} = 0. \end{aligned} \quad (57)$$

The optimization in (57) is then solved using Newton's method with backtracking line search to iteratively update \mathbf{p}_n , c_n , and $g_{m,n}$ until the Karush-Kuhn-Tucker (KKT) conditions are satisfied. This procedure is well-established and can be implemented using commercial software such as MATLAB. We omit the details and denote the solution as $\tilde{\mathbf{p}}_n$.

We iteratively solve (55) and (57) until the maximum number of iterations is reached or the ABAPO scheme converges. The final solutions to the nonconvex optimization in (53) are denoted as $\hat{\mathbf{w}}_k$ and $\hat{\mathbf{p}}_n$.

Remark 5: Note that MMAs can continuously adjust their positions within the transmission region, whereas REMAs are constrained to a set of predefined and discrete positions.

Specifically, MMAs can be regarded as a special case of REMAs when the position interval tends to zero. Thus, the performance of MMAs provides a natural upper bound for evaluating REMA designs. However, characterizing the performance of MMAs involves solving a joint beamforming and antenna positioning optimization problem, which is typically non-convex and challenging to solve. To address this, we propose the ABAPO scheme, which solves the joint optimization problem with an alternating optimization process between beamforming and antenna positioning. The beamforming subproblem has been extensively studied in the literature, while the antenna positioning subproblem can be efficiently addressed using the interior-point method, which is widely supported by commercial solvers such as MATLAB. Owing to its flexibility, the proposed scheme is applicable not only to multiuser communication systems but also to a broader range of system configurations. This enables effective performance characterization of MMAs and facilitates the design and evaluation of REMA-related algorithms.

VI. PERFORMANCE GAP ANALYSIS BETWEEN REMAS AND MMAS

For MMAs, antennas can move continuously within the transmission region, whereas for REMAs, the antenna positions are restricted to discrete locations. As a result, a performance gap arises between REMAs and MMAs, primarily caused by the interval between the candidate radiation positions. This observation leads to a fundamental question: how fine should the position interval be for REMAs to approximate the performance of MMAs? To address this, in this section, we derive the maximum power loss of REMAs compared to MMAs under any given position intervals.

A. Analysis on Power Loss of Electronic Movable Antennas

Suppose the k th user transmits a normalized signal to the BS through the channel given in (2). The received signal at the location $[x_n, 0, z_m]$ is given by

$$\begin{aligned} y &= \sum_{l=1}^{L_k} \sqrt{\frac{1}{N_t}} \gamma_k^{(l)} e^{j2\pi(x_n \cos \phi_k^{(l)} \sin \theta_k^{(l)} + z_m \sin \phi_k^{(l)})/\lambda} \\ &\stackrel{(a)}{=} \sum_{l=1}^{L_k} \sqrt{\frac{1}{N_t}} \gamma_k^{(l)} e^{j2\pi(\Theta_k^{(l)} x_n + \Omega_k^{(l)} z_m)/\lambda}, \end{aligned} \quad (58)$$

where we define $\Theta_k^{(l)} \triangleq \cos \phi_k^{(l)} \sin \theta_k^{(l)}$ and $\Omega_k^{(l)} \triangleq \sin \phi_k^{(l)}$ in (a). With basic trigonometric properties, we have $\Theta_k^{(l)} \in [-1, 1]$ and $\Omega_k^{(l)} \in [-1, 1]$. From (58), we find that the received signal depends on the positions along both the x -axis and z -axis. However, the influence of position changes along these two axes is fundamentally similar. Therefore, we fix the position along the z -axis and focus on variations along the x -axis. Then, we rewrite (58) as

$$y = \sum_{l=1}^{L_k} \tilde{\gamma}_k^{(l)} e^{j2\pi\Theta_k^{(l)} x_n/\lambda}, \quad (59)$$

where the effective channel coefficient $\tilde{\gamma}_k^{(l)}$ is defined as $\tilde{\gamma}_k^{(l)} \triangleq \sqrt{\frac{1}{N_t}} \gamma_k^{(l)} e^{j2\pi\Omega_k^{(l)} z_m/\lambda}$. Note that (59) is structurally

similar to the DTFT but with nonuniform time-domain indices. To convert (59) into the standard DTFT form, we uniformly quantize the angular space $[-1, 1]$ into F discrete samples with the f th sample given by $1 - 2f/F$. Each channel angle $\Theta_k^{(l)}$ is then assigned to its nearest quantized angle, with the corresponding index denoted as \bar{f}_l . Due to the quantization, $\Theta_k^{(l)}$ is not exactly equal to $1 - 2\bar{f}_l/F$. However, as F increases, the quantization error decreases, and $\Theta_k^{(l)}$ converges to $1 - 2\bar{f}_l/F$.

Next, we define an all-zero vector $\mathbf{b} \in \mathbb{C}^F$ and assign values to it as $[\mathbf{b}]_{\bar{f}_l} \leftarrow \tilde{\gamma}_k^{(l)}$. With this definition, (59) can be rewritten as

$$\begin{aligned} y &= \sum_{f=1}^F [\mathbf{b}]_f e^{j2\pi(1-2f/F)x_n/\lambda} \\ &= e^{j2\pi x_n/\lambda} \sum_{f=1}^F [\mathbf{b}]_f e^{-j\pi f \tilde{x}_n}, \end{aligned} \quad (60)$$

where we define $\tilde{x}_n \triangleq \frac{4x_n}{\lambda F}$. From (60), it is evident that y is the DTFT of \mathbf{b} , where \tilde{x}_n represents the frequency domain. According to Fourier analysis [46], the minimum bandwidth of an F -point signal can be approximated using the Dirichlet kernel

$$G_F(\omega) = \left| \frac{\sin(F\omega/2)}{\sin(\omega/2)} \right|. \quad (61)$$

By numerically evaluating (61), the κ -dB bandwidth can be determined as $\Gamma_F^{(\kappa)}$. For example, the minimum 3-dB bandwidth of an F -point signal is approximately $1.76/F$.

On the other hand, since \mathbf{b} contains zeros at unassigned positions, its effective length can be computed as

$$\bar{F} = \left\lceil \frac{(\bar{\Theta}_{\max} - \bar{\Theta}_{\min})F}{2} \right\rceil, \quad (62)$$

where $\bar{\Theta}_{\max} \triangleq \max_l \Theta_k^{(l)}$ and $\bar{\Theta}_{\min} \triangleq \min_l \Theta_k^{(l)}$. Additionally, from (61), we observe that x_n is scaled by a factor of $F\lambda/4$ relative to \tilde{x}_n . Therefore, the κ -dB mainlobe width of y with respect to x_n is given by

$$B^{(\kappa)} = \Gamma_F^{(\kappa)} F\lambda/4. \quad (63)$$

Since $\Gamma_F^{(\kappa)}$ decreases as F increases, a larger interval between the maximum and minimum channel angles results in a smaller mainlobe width of y . Furthermore, $B^{(\kappa)} \geq \Gamma_F^{(\kappa)} F\lambda/4$ due to $\bar{F} \leq F$. Thus, the maximum κ -dB mainlobe width of y with respect to x_n is

$$\bar{B}^{(\kappa)} = \Gamma_F^{(\kappa)} F\lambda/4. \quad (64)$$

Note that (64) establishes a relationship between power loss and position interval. For instance, setting $\kappa = 3$, corresponding to a half-power loss, the position interval is 0.44λ . Conversely, if the position interval is set to 0.2λ , the maximum power loss is computed as 12.5%. In other words, to limit power loss to at most κ dB, the position interval should not exceed $\Gamma_F^{(\kappa)} F\lambda/4$.

B. Evaluation of the Analysis

Now, we validate the analysis in Section VI-A through simulations. We fix the z -axis and change positions along the x -axis within $[-5\lambda, 5\lambda]$. The position interval ranges from 0.5λ to 0.05λ in a step of 0.05λ , resulting in the number of candidate antenna positions varying from 10 to 100. The number of channel paths is set to $L_k = 20$, with channel gains following $\gamma_k^{(l)} \sim \mathcal{CN}(0, 1)$ and channel angles distributed as $\Theta_k^{(l)} \in [-1, 1]$.

Using (64), we determine the position corresponding to the maximum received power for the REMAs. Then, we refine this position using gradient descent to obtain the optimal positions for the MMAs and compute their corresponding maximum received power. Subsequently, the power loss of the REMAs compared to the MMAs can be computed directly.

In Table I, we first calculate the maximum power loss of the REMAs compared to the MMAs using (64). Next, we conduct 10^5 Monte Carlo simulations to obtain the actual power loss of the REMAs relative to the MMAs. Additionally, we compute the ratio of cases where the actual power loss remains below the theoretical maximum given by (64). The results in the table demonstrate that the maximum power loss predicted by our analysis holds in the vast majority of cases, which verifies the accuracy and effectiveness of our analysis for REMAs.

VII. SIMULATION RESULTS

Now, we evaluate the performance of the proposed methods. The width and height of each REMA in the PC-REMAA are set to 1λ .¹ To evaluate the REMAs, we adopt the standard FPAs and MMAs as benchmarks. For a fair comparison, FPAs and MMAs employ the same number of antennas as those selected in the FC-REMAA and PC-REMAA. In addition, the antenna spacing in FPAs is $\lambda/2$, and the transmit region of the MMAs is the same as the antenna panels of the FC-REMAA and PC-REMAA. To evaluate the TS-MBAS scheme, we select two benchmark methods: the flexible precoding (FP) method from [16] and the graph-based approach (GA) from [18]. Both methods are designed for MAs with discrete antenna positions.

Fig. 7 illustrates the sum-rate performance of different methods for various position intervals in a uniform linear array configuration, where $N_r = 1$. The number of candidate antennas in each REMA ranges from 2 to 20, corresponding to the position interval from $\lambda/2$ to $\lambda/20$.² The number of selected antennas is $N_s = 4$, the SNR is set to 10 dB, and the system includes $K = 4$ users, each with $L_k = 6$ channel paths. First, we compare the REMAs with the MMAs and FPAs. From the figure, we observe that MMAs achieve the

¹In [33], an RPA with dimensions of $0.67\lambda \times 0.67\lambda$ is fabricated. By optimizing the internal connections among pixels, it is shown to be equivalent to a standard REMA with a length of 0.5λ and 12 ports. Following the same design methodology, the REMA can be scaled up to $1\lambda \times 1\lambda$ by enlarging the pixel layer and modifying the optimization objective.

²In [33], an REMA with a length of 0.5λ and 12 ports is fabricated, which leads to a position interval of $\lambda/24$. Usually, a finer position interval leads to increased design complexity. Therefore, the REMAs with the setting position intervals are practically realizable.

TABLE I
EVALUATION OF THE EFFECTIVENESS OF THE POWER LOSS ANALYSIS FOR THE REMAS

Position Interval	0.5λ	0.45λ	0.40λ	0.35λ	0.30λ	0.25λ	0.20λ	0.15λ	0.10λ	0.05λ
Maximum Power Loss from (64)	59.47%	51.19%	42.72%	34.34%	26.32%	18.94%	12.49%	7.19%	3.25%	0.82%
Percentage of Cases Satisfying (64)	99.96%	99.85%	99.61%	98.90%	98.51%	98.14%	97.43%	97.07%	96.41%	96.17%

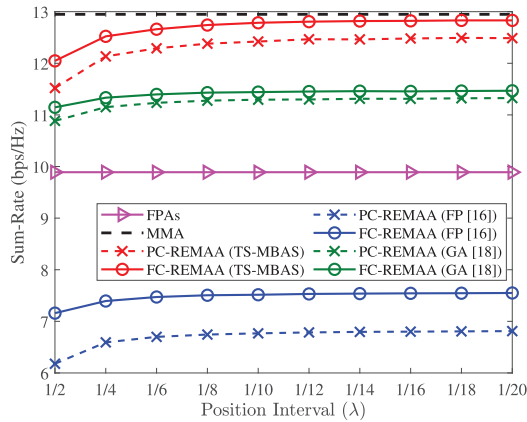


Fig. 7. Comparisons of different methods in terms of the sum-rate for varying position intervals under the uniform linear array configuration.

highest sum-rate, followed by FC-REMAA, PC-REMAA, and FPAs. This performance ordering aligns with the degree of design flexibility in these arrays. Additionally, as the position interval decreases, the FC-REMAA gradually approaches the performance of MMAs. However, reducing the position interval below $\lambda/8$ results in only marginal improvements, which indicates that refining the position interval beyond $\lambda/8$ offers limited practical benefit in enhancing multiuser sum-rate. Then, we compare the TS-MBAS with the FP and GA. From the figure, given the antenna architecture, TS-MBAS achieves the best performance, followed by GA and FP. Notably, FC-REMAA (FP) performs worse than FPAs because FC-REMAA (FP) employs zero-forcing beamforming, whereas FPAs use the superior WMMSE algorithm for multiuser beamforming. TS-MBAS outperforms GA because GA selects antennas solely based on channel gains, while TS-MBAS jointly optimizes antenna selection and beamforming to maximize the multiuser sum-rate. Furthermore, with TS-MBAS, FC-REMAA approaches the performance of MMAs, validating the effectiveness of both FC-REMAA and TS-MBAS.

Fig. 8 extends the analysis in Fig. 7 to a uniform planar array configuration. The number of candidate antennas per row and column in each REMA ranges from 2 to 9, corresponding to the position interval from $\lambda/2$ to $\lambda/9$. The other system parameters are the same as those in Fig. 7. The comparison results of different methods in Fig. 8 are consistent with those in Fig. 7 and therefore are omitted. Comparing the results from Fig. 7 and Fig. 8, we find that the MMAs, FC-REMAA, and PC-REMAA perform better in the planar configuration due to the increased flexibility in antenna placement. In contrast, the

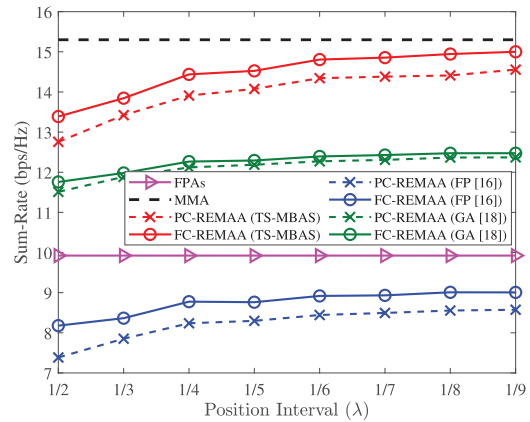


Fig. 8. Comparisons of different methods in terms of the sum-rate for varying position intervals under the uniform planar array configuration.

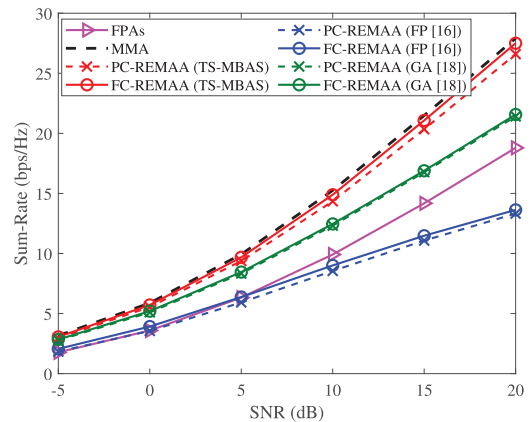


Fig. 9. Comparisons of different methods in terms of the sum-rate for varying SNRs under the uniform planar array configuration.

performance of FPAs remains similar in both figures because the fixed antenna positions limit their adaptability. Furthermore, as the position interval decreases, the FC-REMAA (TS-MBAS) can also gradually approach the performance of MMAs in uniform planar array configurations.

Fig. 9 illustrates the sum-rate performance under varying SNRs, considering a uniform planar array configuration with eight candidate antennas per row and column in each REMA. The number of selected antennas is $N_s = 4$, and the system includes $K = 4$ users, each with $L_k = 6$ channel paths. The results show that the performance gap between MMAs and FC-REMAA (TS-MBAS) widens gradually as the SNR increases, while the gap between FC-REMAA (TS-MBAS)

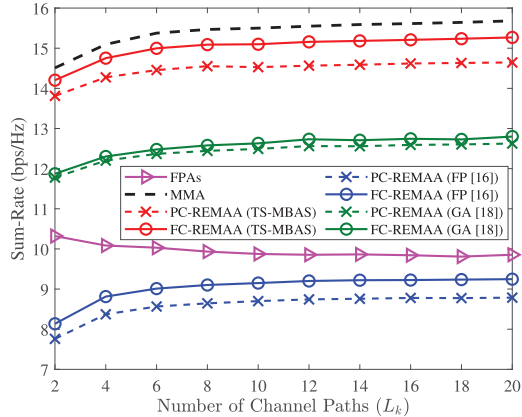


Fig. 10. Comparisons of different methods in terms of the sum-rate for varying numbers of channel paths under the uniform planar array configuration.

and FPAs grows more rapidly. This trend is due to the significantly higher flexibility of FC-REMAA compared to FPAs in antenna position design, which allows for more effective suppression of multiuser interference. As the SNR increases and noise power diminishes, interference becomes the dominant factor affecting performance, making interference mitigation even more critical. Consequently, the advantage of FC-REMAA over FPAs becomes more apparent. However, while MMAs offer even greater flexibility than FC-REMAA, the additional freedom is comparatively limited, leading to a slower performance gain relative to FC-REMAA (TS-MBAS) as the SNR increases. Moreover, FC-REMAA (TS-MBAS) consistently approaches the performance of MMAs across different SNR levels, demonstrating the effectiveness of the proposed approach.

Fig. 10 illustrates the impact of the number of channel paths on sum-rate performance in the uniform planar array configuration. The number of candidate antennas per row and column in an REMA is set to 8, the number of selected antennas is $N_s = 4$, and the SNR remains at 10 dB. From the figure, the performance of MMAs, FC-REMAA, and PC-REMAA improves as the number of channel paths increases because the received power fluctuates more rapidly within the receive region. In this context, these methods can more easily identify favorable antenna positions for multiuser communications. However, the rapid power variation also results in a narrower mainlobe width and greater power loss for FPAs, as analyzed in Section VI, which leads to the decline in performance of FPAs as the number of channel paths increases.

Fig. 11 illustrates the sum-rate performance for varying number of users under a uniform planar array configuration. Each REMA consists of 6 candidate antennas per row and column. The PC-REMAA employs three REMAs per row and two REMAs per column, leading to a total of 18 candidate antennas per row and 12 candidate antennas per column. For fairness, FC-REMAA is configured with the same number of candidate antennas as the PC-REMAA. The number of selected antennas is $N_s = 6$, the SNR is set to 10 dB, and each user has $L_k = 6$ channel paths. The results

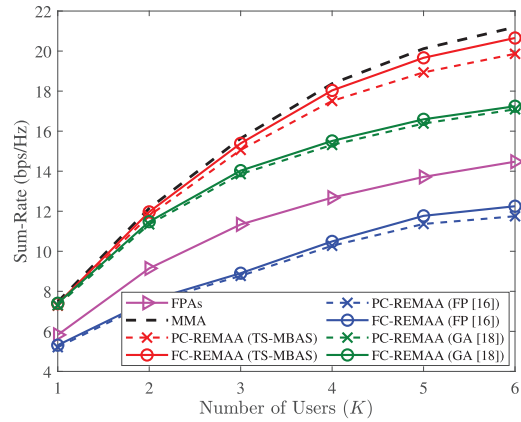


Fig. 11. Comparisons of different methods in terms of the sum-rate for varying numbers of users under the uniform planar array configuration.

show that as the number of users increases, the performance gap between MMAs and FC-REMAA (TS-MBAS) widens gradually, whereas the gap between FC-REMAA (TS-MBAS) and FPAs expands more rapidly. This is because greater antenna position flexibility enhances sum-rate performance, particularly in complicated scenarios with a larger number of users.

Note that the tuning of MMAs relies on motors and syringes, resulting in response times ranging from milliseconds to seconds [47]. This latency renders MMAs unsuitable for tracking rapid channel variations and limits their practical applicability. In contrast, REMAs use RF switches, such as PIN diodes, enabling response times from nanoseconds to milliseconds. These response times are much shorter than typical channel coherence times, making REMAs suitable for practical deployment. Furthermore, simulation results show that the performance of FC-REMAA (TS-MBAS) closely approaches that of MMAs under various conditions. Overall, due to their significantly faster response, lower complexity and comparable performance, REMAs are better suited for practical applications than MMAs.

VIII. CONCLUSION

In this paper, we have investigated REMAs for multiuser communications. We have modeled each REMA as an antenna characterized by a set of predefined and discrete selectable radiation positions within the radiating region. Considering trade-off between performance and cost, we have proposed two types of REMA-based arrays: the PC-REMAA and FC-REMAA. We have formulated a multiuser sum-rate maximization problem subject to power constraint and hardware constraints of the PC-REMAA or FC-REMAA. To solve this problem, we have proposed a TS-MBAS scheme. In addition, we have revisited MMAs with continuously adjustable positions within the transmission region to establish a benchmark for evaluating REMA-enabled multiuser communications. We have analyzed the performance gap between REMAs and MMAs. Specifically, we have transformed the received signal of MMAs into the DTFT of the channel coefficients. Based on Fourier analysis, we have derived the maximum power loss of

REMA compared to MMAs for any given position interval. Future research will focus on further exploring the applications of REMA in wireless communications.

REFERENCES

- [1] K. Chen, C. Qi, Y. Hong, and C. Yuen, "Multiuser sum-rate maximization for reconfigurable pixel antenna-based electronic movable-antenna arrays," in *Proc. IEEE 26th Workshop Signal Process. Artif. Intell. Wireless Commun. (SPAWC)*, Jul. 2025, pp. 1–5.
- [2] P. Yang, Y. Xiao, M. Xiao, and S. Li, "6G wireless communications: Vision and potential techniques," *IEEE Netw.*, vol. 33, no. 4, pp. 70–75, Jul. 2019.
- [3] K. Chen, C. Qi, J. Huang, O. A. Dobre, and G. Y. Li, "Near-field communications for extremely large-scale MIMO: A beamspace perspective," *IEEE Commun. Mag.*, vol. 63, no. 5, pp. 166–172, May 2025.
- [4] T. Rappaport, *Wireless Communications: Principles and Practice*, 2nd ed., Upper Saddle River, NJ, USA: Prentice-Hall, 2001.
- [5] R. W. Heath Jr. and A. J. Paulraj, "Switching between diversity and multiplexing in MIMO systems," *IEEE Trans. Commun.*, vol. 53, no. 6, pp. 962–968, Jun. 2005.
- [6] L. Lu, G. Y. Li, A. L. Swindlehurst, A. Ashikhmin, and R. Zhang, "An overview of massive MIMO: Benefits and challenges," *IEEE J. Sel. Topics Signal Process.*, vol. 8, no. 5, pp. 742–758, Oct. 2014.
- [7] Z. Wang, J. Zhang, E. Björnson, D. Niyato, and B. Ai, "Optimal bilinear equalizer for cell-free massive MIMO systems over correlated Rician channels," *IEEE Trans. Signal Process.*, early access, Mar. 11, 2025, doi: [10.1109/TSP.2025.3547380](https://doi.org/10.1109/TSP.2025.3547380).
- [8] C. Qi, K. Chen, O. A. Dobre, and G. Y. Li, "Hierarchical codebook-based multiuser beam training for millimeter wave massive MIMO," *IEEE Trans. Wireless Commun.*, vol. 19, no. 12, pp. 8142–8152, Dec. 2020.
- [9] E. Ali, M. Ismail, R. Nordin, and N. F. Abdulah, "Beamforming techniques for massive MIMO systems in 5G: Overview, classification, and trends for future research," *Frontiers Inf. Technol. Electron. Eng.*, vol. 18, no. 6, pp. 753–772, Jun. 2017.
- [10] K. Chen, C. Qi, G. Y. Li, and O. A. Dobre, "Near-field multiuser communications based on sparse arrays," *IEEE J. Sel. Topics Signal Process.*, vol. 18, no. 4, pp. 619–632, May 2024.
- [11] C. Qi, J. Hu, Y. Du, and A. Nallanathan, "Multiuser beamforming for partially-connected millimeter wave massive MIMO," *IEEE Trans. Veh. Technol.*, vol. 73, no. 4, pp. 5977–5981, Apr. 2024.
- [12] S. Sanayei and A. Nosratinia, "Antenna selection in MIMO systems," *IEEE Commun. Mag.*, vol. 42, no. 10, pp. 68–73, Oct. 2004.
- [13] A. Molisch, M. Win, Y.-S. Choi, and J. Winters, "Capacity of MIMO systems with antenna selection," *IEEE Trans. Wireless Commun.*, vol. 4, no. 4, pp. 1759–1772, Jul. 2005.
- [14] S. Asaad, A. M. Rabiei, and R. R. Müller, "Massive MIMO with antenna selection: Fundamental limits and applications," *IEEE Trans. Wireless Commun.*, vol. 17, no. 12, pp. 8502–8516, Dec. 2018.
- [15] L. Zhu and K.-K. Wong, "Historical review of fluid antenna and movable antenna," 2024, *arXiv:2401.02362*.
- [16] S. Yang, W. Lyu, B. Ning, Z. Zhang, and C. Yuen, "Flexible precoding for multi-user movable antenna communications," *IEEE Wireless Commun. Lett.*, vol. 13, no. 5, pp. 1404–1408, May 2024.
- [17] B. Feng, Y. Wu, X.-G. Xia, and C. Xiao, "Weighted sum-rate maximization for movable antenna-enhanced wireless networks," *IEEE Wireless Commun. Lett.*, vol. 13, no. 6, pp. 1770–1774, Jun. 2024.
- [18] W. Mei, X. Wei, B. Ning, Z. Chen, and R. Zhang, "Movable-antenna position optimization: A graph-based approach," *IEEE Wireless Commun. Lett.*, vol. 13, no. 7, pp. 1853–1857, Apr. 2024.
- [19] J. An, C. Yuen, M. D. Renzo, M. Debbah, H. V. Poor, and L. Hanzo, "Flexible intelligent metasurfaces for downlink multiuser MISO communications," *IEEE Trans. Wireless Commun.*, vol. 24, no. 4, pp. 2940–2955, Apr. 2025.
- [20] J. An, C. Yuen, M. Debbah, and L. Hanzo, "Flexible intelligent metasurfaces for enhanced MIMO communications," in *Proc. IEEE Int. Conf. Commun. (ICC)*, Montreal, QC, Canada, Jun. 2025, pp. 1–6.
- [21] L. Zhu, W. Ma, and R. Zhang, "Modeling and performance analysis for movable antenna enabled wireless communications," *IEEE Trans. Wireless Commun.*, vol. 23, no. 6, pp. 6234–6250, Jun. 2024.
- [22] K.-K. Wong, A. Shojaeifard, K.-F. Tong, and Y. Zhang, "Fluid antenna systems," *IEEE Trans. Wireless Commun.*, vol. 20, no. 3, pp. 1950–1962, Mar. 2021.
- [23] H. Xu et al., "Capacity maximization for FAS-assisted multiple access channels," *IEEE Trans. Commun.*, vol. 73, no. 7, pp. 4713–4731, Jul. 2025.
- [24] W. Ma, L. Zhu, and R. Zhang, "MIMO capacity characterization for movable antenna systems," *IEEE Trans. Wireless Commun.*, vol. 23, no. 4, pp. 3392–3407, Apr. 2024.
- [25] L. Zhu, W. Ma, B. Ning, and R. Zhang, "Movable-antenna enhanced multiuser communication via antenna position optimization," *IEEE Trans. Wireless Commun.*, vol. 23, no. 7, pp. 7214–7229, Jul. 2024.
- [26] Y. Wu, D. Xu, D. W. K. Ng, W. Gerstacker, and R. Schober, "Movable antenna-enhanced multiuser communication: Jointly optimal discrete antenna positioning and beamforming," in *Proc. GLOBECOM - IEEE Global Commun. Conf.*, Kuala Lumpur, Malaysia, Dec. 2023, pp. 1–6.
- [27] Y. Wu, D. Xu, D. Wing Kwan Ng, W. Gerstacker, and R. Schober, "Globally optimal movable antenna-enhanced multiuser communication: Discrete antenna positioning, motion power consumption, and imperfect CSI," 2024, *arXiv:2408.15435*.
- [28] W. Ma, L. Zhu, and R. Zhang, "Movable antenna enhanced wireless sensing via antenna position optimization," *IEEE Trans. Wireless Commun.*, vol. 23, no. 11, pp. 16575–16589, Nov. 2024.
- [29] W. Ma, L. Zhu, and R. Zhang, "Movable antenna enhanced integrated sensing and communication via antenna position optimization," 2025, *arXiv:2501.07318*.
- [30] W. Lyu, S. Yang, Y. Xiu, Z. Zhang, C. Assi, and C. Yuen, "Movable antenna enabled integrated sensing and communication," *IEEE Trans. Wireless Commun.*, vol. 24, no. 4, pp. 2862–2875, Apr. 2025.
- [31] G. Hu, Q. Wu, K. Xu, J. Si, and N. Al-Dhahir, "Secure wireless communication via movable-antenna array," *IEEE Signal Process. Lett.*, vol. 31, pp. 516–520, 2024.
- [32] C. Zhou, B. Lyu, C. You, and Z. Liu, "Movable antenna enabled symbiotic radio systems: An opportunity for mutualism," *IEEE Wireless Commun. Lett.*, vol. 13, no. 10, pp. 2752–2756, Oct. 2024.
- [33] J. Zhang et al., "A novel pixel-based reconfigurable antenna applied in fluid antenna systems with high switching speed," *IEEE Open J. Antennas Propag.*, vol. 6, no. 1, pp. 212–228, Feb. 2025.
- [34] K. Chen, C. Qi, and O. A. Dobre, "DBRAA: Sub-6 GHz and millimeter wave dual-band reconfigurable antenna array for ISAC," *IEEE Trans. Commun.*, early access, May 5, 2025, doi: [10.1109/TCOMM.2025.3567007](https://doi.org/10.1109/TCOMM.2025.3567007).
- [35] S. Song and R. D. Murch, "An efficient approach for optimizing frequency reconfigurable pixel antennas using genetic algorithms," *IEEE Trans. Antennas Propag.*, vol. 62, no. 2, pp. 609–620, Feb. 2014.
- [36] L. Jing, M. Li, and R. Murch, "Compact pattern reconfigurable pixel antenna with diagonal pixel connections," *IEEE Trans. Antennas Propag.*, vol. 70, no. 10, pp. 8951–8961, Oct. 2022.
- [37] C. Qi, Q. Liu, X. Yu, and G. Y. Li, "Hybrid precoding for mixture use of phase shifters and switches in mmWave massive MIMO," *IEEE Trans. Commun.*, vol. 70, no. 6, pp. 4121–4133, Jun. 2022.
- [38] W. Ma, L. Zhu, and R. Zhang, "Compressed sensing based channel estimation for movable antenna communications," *IEEE Commun. Lett.*, vol. 27, no. 10, pp. 2747–2751, Oct. 2023.
- [39] Z. Xiao et al., "Channel estimation for movable antenna communication systems: A framework based on compressed sensing," *IEEE Trans. Wireless Commun.*, vol. 23, no. 9, pp. 11814–11830, Sep. 2024.
- [40] H. Xu et al., "Channel estimation for FAS-assisted multiuser mmWave systems," *IEEE Commun. Lett.*, vol. 28, no. 3, pp. 632–636, Mar. 2024.
- [41] J. Lee and S. Leyffer, *Mixed Integer Nonlinear Programming*. New York, NY, USA: Springer, 2011.
- [42] X. Zhao, S. Lu, Q. Shi, and Z.-Q. Luo, "Rethinking WMMSE: Can its complexity scale linearly with the number of BS antennas?," *IEEE Trans. Signal Process.*, vol. 71, pp. 433–446, 2023.
- [43] Q. Shi, W. Xu, J. Wu, E. Song, and Y. Wang, "Secure beamforming for MIMO broadcasting with wireless information and power transfer," *IEEE Trans. Wireless Commun.*, vol. 14, no. 5, pp. 2841–2853, May 2015.
- [44] R. Liu, M. Li, Q. Liu, and A. L. Swindlehurst, "DOA estimation-oriented joint array partitioning and beamforming designs for ISAC systems," *IEEE Trans. Wireless Commun.*, vol. 24, no. 3, pp. 2052–2066, Mar. 2025.
- [45] R. A. Waltz, J. L. Morales, J. Nocedal, and D. Orban, "An interior algorithm for nonlinear optimization that combines line search and trust region steps," *Math. Program.*, vol. 107, no. 3, pp. 391–408, Jul. 2006.
- [46] G. B. Folland, *Fourier Analysis and Its Applications*. Providence, RI, USA: American Mathematical Society, 1992.
- [47] L. Zhu et al., "A tutorial on movable antennas for wireless networks," *IEEE Commun. Surveys Tuts.*, early access, Feb. 27, 2025, doi: [10.1109/COMST.2025.3546373](https://doi.org/10.1109/COMST.2025.3546373).



Kangjian Chen (Graduate Student Member, IEEE) received the B.S. degree from Nanjing University of Science and Technology, Nanjing, China, in 2017, and the M.S. degree in signal processing from Southeast University, Nanjing, in 2020, where he is currently pursuing the Ph.D. degree. His current research interests include integrated sensing and communication (ISAC), massive MIMO, and reconfigurable intelligent surface (RIS). He received the Best Paper Award from IEEE Global Communications Conference (GLOBECOM) in 2019 and

IEEE/CIC International Conference on Communications in China (ICCC) in 2022.



Yujing Hong (Graduate Student Member, IEEE) received the B.S. degree in electronic information science and technology from the University of Electronic Science and Technology of China (UESTC), Chengdu, China, in 2021, and the M.Sc. degree in communications engineering from Nanyang Technological University (NTU), Singapore, in 2023, where he is currently pursuing the Ph.D. degree. His research interests include reconfigurable intelligent surfaces, angle-selective surfaces, and phased array antennas.



Chau Yuen (Fellow, IEEE) received the B.Eng. and Ph.D. degrees from Nanyang Technological University, Singapore, in 2000 and 2004, respectively. He was a Post-Doctoral Fellow with Lucent Technologies Bell Laboratories, Murray Hill, in 2005. From 2006 to 2010, he was with the Institute for Infocomm Research, Singapore. From 2010 to 2023, he was with the Engineering Product Development Pillar, Singapore University of Technology and Design. Since 2023, he has been with the School of Electrical and Electronic Engineering, Nanyang Technological University. Currently, he is the Provost's Chair of wireless communications, the Assistant Dean of the Graduate College, and the Cluster Director of Sustainable Built Environment at ER@IN. He has four U.S. patents and published more than 500 research articles in international journals.

Dr. Yuen received the IEEE Communications Society Leonard G. Abraham Prize in 2024, the IEEE Communications Society Best Tutorial Paper Award in 2024, the IEEE Communications Society Fred W. Ellersick Prize in 2023, the IEEE Marconi Prize Paper Award in Wireless Communications in 2021, the IEEE APB Outstanding Paper Award in 2023, and the EURASIP Best Paper Award for *Journal on Wireless Communications and Networking* in 2021. He serves as the Editor-in-Chief for *Computer Science* (Springer Nature); and an Editor for IEEE TRANSACTIONS ON VEHICULAR TECHNOLOGY, IEEE TRANSACTIONS ON NEURAL NETWORKS AND LEARNING SYSTEMS, and IEEE TRANSACTIONS ON NETWORK SCIENCE AND ENGINEERING, where he was awarded as the IEEE Transactions on Network Science and Engineering Excellent Editor Award in 2022 and 2024, and a Top Associate Editor for IEEE TRANSACTIONS ON VEHICULAR TECHNOLOGY from 2009 to 2015. He also served as a Guest Editor for several special issues, including IEEE JOURNAL ON SELECTED AREAS IN COMMUNICATIONS, *IEEE Wireless Communications Magazine*, *IEEE Communications Magazine*, *IEEE Vehicular Technology Magazine*, IEEE TRANSACTIONS ON COGNITIVE COMMUNICATIONS AND NETWORKING, and *Applied Energy* (Elsevier). He has been listed as a Top 2% Scientist by Stanford University, and also a Highly Cited Researcher by Clarivate Web of Science since 2022.



Chenhao Qi (Senior Member, IEEE) received the B.S. degree (Hons.) in information engineering from the Chien-Shiung Wu Honored College, Southeast University, China, in 2004, and the Ph.D. degree in signal and information processing from Southeast University in 2010.

From 2008 to 2010, he visited the Department of Electrical Engineering, Columbia University, New York, USA. Since 2010, he has been a Faculty Member with the School of Information Science and Engineering, Southeast University, where he is currently a Professor and the Head of Jiangsu Multimedia Communication and Sensing Technology Research Center. He received the Best Paper Award from IEEE GLOBECOM in 2019, IEEE/CIC ICC in 2022, and the 11th International Conference on Wireless Communications and Signal Processing (WCSP) in 2019. He has served as an Associate Editor for IEEE TRANSACTIONS ON COMMUNICATIONS, IEEE COMMUNICATIONS LETTERS, IEEE OPEN JOURNAL OF THE COMMUNICATIONS SOCIETY, IEEE OPEN JOURNAL OF VEHICULAR TECHNOLOGY, and *China Communications*.